

Form factors for semileptonic, nonleptonic and rare $B(B_s)$ meson decays

Mikhail A. Ivanov,¹ Jürgen G. Körner,² Sergey G. Kovalenko,³ Pietro Santorelli,⁴ and Gozyl G. Saidullaeva⁵

¹*Bogoliubov Laboratory of Theoretical Physics,
Joint Institute for Nuclear Research, 141980 Dubna, Russia*

²*Institut für Physik, Johannes Gutenberg-Universität,
D-55099 Mainz, Germany*

³*Centro de Estudios Subatómicos (CES), Universidad Técnica Federico Santa María,
Casilla 110-V, Valparaíso, Chile*

⁴*Dipartimento di Scienze Fisiche, Università di Napoli Federico II,
Complesso Universitario di Monte S. Angelo, Via Cintia, Edificio 6,*

80126 Napoli, Italy, and Istituto Nazionale di Fisica Nucleare, Sezione di Napoli

⁵*Al-Farabi Kazak National University, 480012 Almaty, Kazakhstan*

We provide new values for the model parameters of the covariant constituent quark model (with built-in infrared confinement) in the meson sector by a fit to the leptonic decay constants and a number of electromagnetic decays. We then evaluate, in a parameter-free way, the form factors of the $B(B_s) \rightarrow P(V)$ transitions in the full kinematical region of momentum transfer. As an application of our results we calculate the widths of the nonleptonic B_s -decays into $D_s^- D_s^+$, $D_s^{*-} D_s^+ + D_s^- D_s^{*+}$ and $D_s^{*-} D_s^{*+}$. These modes give the largest contribution to $\Delta\Gamma$ for the $B_s - \bar{B}_s$ system. We also treat the nonleptonic decay $B_s \rightarrow J/\psi\phi$. Although this mode is color-suppressed, this decay has important implications for the search of possible CP-violating new physics effects in $B_s - \bar{B}_s$ mixing.

PACS numbers: 13.20.He, 12.39.Ki

Keywords:

I. INTRODUCTION

The study of heavy flavor physics is important due to the unique possibility of determining the Cabibbo-Kobayashi-Maskawa matrix elements. Such studies also provide insights into the origin of flavor and CP-violation. Moreover, one of the main purposes of heavy-flavor experiments is to look for new physics beyond the standard model (see the recent review [1]). The subject to study are heavy hadrons containing a b - or a c -quark and their weak decays. Note that the t quark decays too quickly to form stable hadrons. Recently, time-dependent measurements of CP violation in the $B_s - \bar{B}_s$ system have become available. In the wake of these measurements, the decay $B_s \rightarrow J/\psi\phi$ has attracted much attention from both theorists and experimentalists (see, for instance, Refs. [2, 3] and references therein).

The main idea in the theoretical studies of heavy-flavor decays is to separate short-distance (perturbative) QCD dynamics from long-distance (nonperturbative) hadronic effects. One uses the so-called *naive* factorization approach which is based on the weak effective Hamiltonian describing quark and lepton transitions in terms of local operators that are multiplied by Wilson coefficients (for a review, see Ref. [4]). The Wilson coefficients characterize the short-distance dynamics and may be reliably evaluated by perturbative methods. The calculation of the hadronic matrix elements of local operators between initial and final states require nonperturbative methods. One needs to know how hadrons are constructed from quarks. Technically, any matrix element of a local operator may be expressed in terms of a set of scalar functions which are referred to as form factors. The so-called QCD factorization and the soft-collinear effective theory yield factorization theorems which allow for a systematic description of a given process in terms of products of soft and hard matrix elements (we refer an interested reader to Refs. [5], [6] and [7]).

A variety of theoretical approaches have been used to evaluate the hadronic form factors. The least model dependent among these is the light-cone sum rule (LCSR) approach (see Refs. [8] and [9]). In the LCSR approach one can access the form factors in the large recoil (small momentum transfer) region which are then extrapolated to the near-zero recoil region using some model-dependent pole-type parametrizations. Grinstein and Pirjol have developed a systematic approach to the rare decay $B \rightarrow K^* \ell^+ \ell^-$ in the low recoil region using the heavy-quark effective theory framework [10]. The low-recoil approach was later studied in detail in Ref. [11].

We mention a few other model approaches for the calculation of the form factors. They are based on the study of i) Dyson-Schwinger equations in QCD [12]; ii) the constituent quark model using dispersion relations [13]; iii) a relativistic quark model developed by Ebert, Faustov and Galkin [14]; iv) a QCD relativistic potential model [15] (see also [16]); v) a QCD sum rule analysis [17]; and, finally, vi) the covariant constituent quark model developed by some of us starting with Refs. [18], [19] and [20]. It is worth mentioning that the entire physical range of momentum

transfer is accessible in the covariant quark model approach used in Refs. [18–20] and the present paper and in the calculations of Refs. [12–15, 17].

The earlier versions of the covariant constituent quark model (for short: covariant quark model [39]) in Refs. [18–20] did not include the confinement of quarks. The nonconfined version had been applied, among others, to the description of B and B_c transition form factors using a small set of model parameters. In the covariant quark model, meson transitions are described by covariant Feynman diagrams with free constituent quark propagation. The ultraviolet behavior of the loop diagrams is tempered by appropriately damped vertex functions. A key role in the consistent formulation of the model is played by the so-called compositeness condition [21, 22], a corollary of which guarantees the correct charge normalization of charged mesons at zero momentum transfer. Since the propagation of the constituent quarks is described by free-particle Green's functions, one will encounter on-shell quark production in the case when the mass of the bound state exceeds the sum of the constituent quark masses. Therefore, the applicability of the covariant quark model in its original version was limited to the cases where $m_H < m_{q_1} + m_{q_2}$. This limitation was removed later on in Ref. [23] by effectively introducing infrared confinement through the introduction of a universal infrared cutoff parameter in the space of loop integrations. This extended the applicability of the covariant quark model to all processes involving heavy and light hadrons. The viability of the improved covariant quark model was demonstrated in a number of applications to mesonic transitions in Ref. [23]. Later on, this approach was successfully applied to a study of the tetraquark state $X(3872)$ and its strong and radiative decays (see Refs. [24, 25]).

Once the parameters of the covariant quark model have been determined the covariant quark model is a very flexible tool that can be used to calculate any heavy-to-heavy, heavy-to-light and light-to-light hadron transition. While the more model independent approaches usually have to rely on a heavy quark mass expansion the predictions of the covariant quark model hold for general mass configurations which are not accessible to the model-independent approaches. On the other hand the predictions of the heavy-quark expansion can be recovered by using static propagators for the heavy quarks.

In this paper we use the improved version of the covariant quark model including infrared confinement to evaluate the form factors of the $B(B_s) \rightarrow P(V)$ transitions in the full kinematical range of momentum transfer. As an application of our results we calculate the widths of several B_s nonleptonic decays. These are the modes $B_s \rightarrow D_s^- D_s^+, D_s^{*-} D_s^{*+} + D_s^- D_s^{*+}$, and $B_s \rightarrow D_s^{*-} D_s^{*+}$ which give the largest contribution to $\Delta\Gamma$ for the $B_s - \bar{B}_s$ system. We also treat the color-suppressed mode $B_s \rightarrow J/\psi\phi$. This decay is important for the search of possible CP-violating new physics effects in $B_s - \bar{B}_s$ mixing.

Our paper is structured as follows. In Sec. II, we give a brief sketch of the theoretical framework underlying the covariant quark model including a discussion of how infrared confinement is set up in the loop integrations. In Sec. III, we discuss in some detail how the model parameters of the covariant quark model are determined through a least-squares fit to experimental/theoretical data on leptonic decay constants and to eight fundamental mesonic one- and two-photon decays. Once the model parameters of the covariant quark model are fixed, the model can be used to obtain parameter-free predictions for any transition process involving light or heavy mesons. In Sec. IV, we calculate the transition form factors of the B and B_s mesons to light pseudoscalar and vector mesons which are needed as ingredients for the calculation of the semileptonic, nonleptonic and rare decays of the B and B_s mesons. In Sec. V, we make use of the calculated form factors to calculate the nonleptonic decays $B_s \rightarrow D_s^{(*)-} D_s^{(*)+}$ and $B_s \rightarrow J/\psi\phi$ which have recently attracted some attention as explained above. Finally, in Sec. VI, we summarize our findings.

II. EFFECTIVE LAGRANGIANS, COMPOSITENESS CONDITION, AND INFRARED CONFINEMENT

In this section, we give a brief description of the theoretical framework underlying the formulation of the covariant quark model. We first define a nonlocal meson-quark-quark vertex in terms of an effective Lagrangian. We then introduce the compositeness condition and discuss its significance. We then, finally, describe how infrared confinement is incorporated into the model. This involves a technical discussion of how the one-loop integrations are done, which we briefly describe.

The coupling of a meson $H(q_1\bar{q}_2)$ to its constituent quarks q_1 and \bar{q}_2 is described by the effective Lagrangian [26, 27]

$$\mathcal{L}_{\text{int Hqq}}(x) = g_H H(x) \int dx_1 \int dx_2 F_H(x, x_1, x_2) \bar{q}_2(x_2) \Gamma_H q_1(x_1) + \text{h.c.} \quad (1)$$

Γ_H is a Dirac matrix or a string of Dirac matrices which projects onto the spin quantum number of the meson field $H(x)$. In the present case, the Dirac structures involved are γ_5 for the pseudoscalar meson and γ_μ for the vector meson. The function F_H is related to the scalar part of the Bethe-Salpeter amplitude and characterizes the finite size of the meson. To satisfy translational invariance, the scalar function F_H has to fulfill the relation

$F_H(x+a, x_1+a, x_2+a) = F_H(x, x_1, x_2)$ for any four-vector a . A specific form which satisfies translational invariance is the form

$$F_H(x, x_1, x_2) = \delta(x - w_1 x_1 - w_2 x_2) \Phi_H((x_1 - x_2)^2) \quad (2)$$

where Φ_H is the correlation function of the two constituent quarks with masses m_{q_1} , m_{q_2} , and the mass ratios $w_i = m_{q_i}/(m_{q_1} + m_{q_2})$.

The coupling constant g_H in Eq. (1) is constrained by the so-called *compositeness condition* originally proposed in Refs. [21, 22], and extensively used in Refs. [26, 27]. The compositeness condition requires that the renormalization constant of the elementary meson field $H(x)$ is set to zero:

$$Z_H = 1 - \frac{3g_H^2}{4\pi^2} \tilde{\Pi}'_H(m_H^2) = 0 \quad (3)$$

where $\tilde{\Pi}'_H$ is the derivative of the meson mass operator.

To clarify the physical meaning of the compositeness condition in Eq. (3), we first want to remind the reader that the renormalization constant $Z_H^{1/2}$ can also interpreted as the matrix element between the physical and the corresponding bare state. The condition $Z_H = 0$ implies that the physical state does not contain the bare state and is appropriately described as a bound state. The interaction Lagrangian of Eq. (1) and the corresponding free parts of the Lagrangian describe both the constituents (quarks) and the physical particles (hadrons) which are viewed as the bound states of the quarks. As a result of the interaction, the physical particle is dressed, i.e. its mass and wave function have to be renormalized.

In a more familiar setting the compositeness condition $Z_H = 0$ guarantees the correct charge normalization of a charged particle at zero momentum transfer. This can be seen by using an identity relating the derivative of the free-quark propagator (with loop momentum $k+p$) with the electromagnetic γ_μ coupling to the same propagator at zero momentum transfer. The identity reads

$$\frac{\partial}{\partial p^\mu} \frac{1}{m_q - \not{k} - \not{p}} = \frac{1}{m_q - \not{k} - \not{p}} \gamma_\mu \frac{1}{m_q - \not{k} - \not{p}}. \quad (4)$$

The contribution of the left-hand-side of Eq.(4) is normalized due to the compositeness condition, and, therefore, the contribution of the right-hand-side is also normalized.

The condition $Z_H = 0$ also effectively excludes the constituent degrees of freedom from the space of physical states. It thereby guarantees that there is no double counting for the physical observable under consideration. The constituents exist only in virtual states. One of the corollaries of the compositeness condition is the absence of a direct interaction of the dressed charged particle with the electromagnetic field. Taking into account both the tree-level diagram and the diagrams with self-energy insertions into the external legs (i.e. the tree-level diagram times $Z_H - 1$) yields a common factor Z_H , which is equal to zero. We refer the interested reader to our previous papers [19, 26, 27] where these points are discussed in more detail.

In the case of pseudoscalar and vector mesons, the derivative of the meson mass operator appearing in Eq. (3) can be calculated from the one-loop two-point function given by

$$\begin{aligned} \tilde{\Pi}'_P(p^2) &= \frac{1}{2p^2} p^\alpha \frac{d}{dp^\alpha} \int \frac{d^4 k}{4\pi^2 i} \tilde{\Phi}_P^2(-k^2) \text{tr} \left[\gamma^5 S_1(k + w_1 p) \gamma^5 S_2(k - w_2 p) \right] \\ &= \frac{1}{2p^2} \int \frac{d^4 k}{4\pi^2 i} \tilde{\Phi}_P^2(-k^2) \left\{ w_1 \text{tr} \left[\gamma^5 S_1(k + w_1 p) \not{p} S_1(k + w_1 p) \gamma^5 S_2(k - w_2 p) \right] \right. \\ &\quad \left. - w_2 \text{tr} \left[\gamma^5 S_1(k + w_1 p) \gamma^5 S_2(k - w_2 p) \not{p} S_2(k - w_2 p) \right] \right\} \\ \tilde{\Pi}'_V(p^2) &= \frac{1}{3} \left(g_{\mu\nu} - \frac{p_\mu p_\nu}{p^2} \right) \frac{1}{2p^2} p^\alpha \frac{d}{dp^\alpha} \int \frac{d^4 k}{4\pi^2 i} \tilde{\Phi}_V^2(-k^2) \text{tr} \left[\gamma^\mu S_1(k + w_1 p) \gamma^\nu S_2(k - w_2 p) \right] \\ &= \frac{1}{3} \left(g_{\mu\nu} - \frac{p_\mu p_\nu}{p^2} \right) \frac{1}{2p^2} \int \frac{d^4 k}{4\pi^2 i} \tilde{\Phi}_V^2(-k^2) \left\{ w_1 \text{tr} \left[\gamma^\mu S_1(k + w_1 p) \not{p} S_1(k + w_1 p) \gamma^\nu S_2(k - w_2 p) \right] \right. \\ &\quad \left. - w_2 \text{tr} \left[\gamma^\mu S_1(k + w_1 p) \gamma^\nu S_2(k - w_2 p) \not{p} S_2(k - w_2 p) \right] \right\}, \quad (5) \end{aligned}$$

where $\tilde{\Phi}_H(-k^2)$ is the Fourier-transform of the vertex function $\Phi_H((x_1 - x_2)^2)$, $S_i(k)$ is the free-quark propagator given by

$$S_i(k) = \frac{1}{m_{q_i} - \not{k}}, \quad (6)$$

and m_{q_i} is the effective constituent quark mass m_{q_i} .

For calculational convenience, we will choose a simple Gaussian form for the vertex function $\tilde{\Phi}_H(-k^2)$. One has

$$\tilde{\Phi}_H(-k^2) = \exp(k^2/\Lambda_H^2) \quad (7)$$

where the parameter Λ_H characterizes the size of the respective bound state meson H . Since k^2 turns into $-k_E^2$ in Euclidean space, the form (7) has the appropriate fall-off behavior in the Euclidean region. We emphasize that any choice for Φ_H is appropriate as long as it falls off sufficiently quickly in the ultraviolet region of Euclidean space to render the corresponding Feynman diagrams ultraviolet finite.

The technical details of how the one-loop integrations such as in Eq.(5) are done can be found in Ref. [23]. Let us mention that we use the Schwinger representation to write the local quark propagators as

$$S(k) = (m + \not{k}) \int_0^\infty d\beta e^{-\beta(m^2 - k^2)}. \quad (8)$$

The loop momentum now appears in the exponent which allows one to deal very efficiently with tensor loop integrals by converting loop momenta into derivatives via the identity

$$k_i^\mu e^{2kr} = \frac{1}{2} \frac{\partial}{\partial r_{i\mu}} e^{2kr}, \quad (9)$$

We have written a FORM [28] program that achieves the necessary commutations of the differential operators in a very efficient way.

After doing the loop integration one obtains

$$\Pi = \int_0^\infty d^n \beta F(\beta_1, \dots, \beta_n), \quad (10)$$

for a given Feynman diagram Π , where F stands for the whole structure of a given diagram. For the mass operators of Eq. (5) one has three propagators, and, thus, one has three Schwinger parameters β_i ($i = 1, 2, 3$). For the transition form factors to be discussed later on, one has again three propagators leading again to $n = 3$.

Next, we briefly describe how infrared confinement is implemented [23] in the quark loops. First, note that the set of Schwinger parameters β_i can be turned into a simplex by introducing an additional t integration via the identity

$$1 = \int_0^\infty dt \delta(t - \sum_{i=1}^n \beta_i) \quad (11)$$

leading to

$$\Pi = \int_0^\infty dt t^{n-1} \int_0^1 d^n \alpha \delta\left(1 - \sum_{i=1}^n \alpha_i\right) F(t\alpha_1, \dots, t\alpha_n). \quad (12)$$

There are now altogether n numerical integrations: $(n-1)$ α -parameter integrations and the integration over the scale parameter t . The very large t region corresponds to the region where the singularities of the diagram with its local quark propagators start appearing. However, as described in Ref. [23], if one introduces an infrared cut-off on the upper limit of the t integration, all singularities vanish because the integral is now analytic for any value of the kinematic variables. We cutoff the upper integration at $1/\lambda^2$ and obtain

$$\Pi^c = \int_0^{1/\lambda^2} dt t^{n-1} \int_0^1 d^n \alpha \delta\left(1 - \sum_{i=1}^n \alpha_i\right) F(t\alpha_1, \dots, t\alpha_n). \quad (13)$$

By introducing the infrared cutoff one has removed all potential thresholds in the quark-loop diagram, i.e. the quarks are never on-shell and are thus effectively confined. We take the cutoff parameter λ to be the same in all physical processes, i.e. the infrared parameter is universal. The numerical evaluation of the integrals have been done by a numerical program written in FORTRAN code.

TABLE I: Input values for the leptonic decay constants f_H (in MeV) and our least-squares fit values.

Fit Values	Other	Ref.	This work	Other	Ref.
f_π	128.7	130.4 ± 0.2 [29, 30]	f_ω	198.5	198 ± 2 [29]
f_K	156.1	156.1 ± 0.8 [29, 30]	f_ϕ	228.2	227 ± 2 [29]
f_D	205.9	206.7 ± 8.9 [29, 30]	$f_{J/\psi}$	415.0	415 ± 7 [29]
f_{D_s}	257.5	257.5 ± 6.1 [29, 30]	f_{K^*}	213.7	217 ± 7 [29]
f_B	191.1	192.8 ± 9.9 [31]	f_{D^*}	243.3	245 ± 20 [33]
f_{B_s}	234.9	238.8 ± 9.5 [31]	$f_{D_s^*}$	272.0	272 ± 26 [33]
f_{B_c}	489.0	489 ± 5 [32]	f_{B^*}	196.0	196 ± 44 [33]
f_ρ	221.1	221 ± 1 [29]	$f_{B_s^*}$	229.0	229 ± 46 [33]

III. MODEL PARAMETERS

Let us first enumerate the number of model parameters in the covariant quark model. For a given meson H_i these are the coupling parameter g_{H_i} , the size parameter Λ_{H_i} , two of the four effective constituent quark masses m_{q_j} ($m_u = m_d, m_s, m_c, m_b$), and the universal confinement parameter λ . For n_H mesons one therefore has $2n_H + 5$ model parameters. The compositeness condition provides n_H constraints on the model parameters, which we symbolically write as

$$f_{H_i}(g_{H_i}, \Lambda_{H_i}, m_{q_i}, \lambda) = 1 \quad (14)$$

The constraint (14) can be used, e.g., to eliminate the coupling parameter g_H from the set of parameters. The remaining parameters are determined by a fit to experimental data. An obvious choice is to fit the model parameters to the experimental values of the leptonic decay constants. In the covariant quark model the relevant expressions for the pseudoscalar and vector mesons are given by

$$\begin{aligned} N_c g_P \int \frac{d^4 k}{(2\pi)^4 i} \tilde{\Phi}_P(-k^2) \text{tr} \left[O_P^\mu S_1(k + w_1 p) \gamma^5 S_2(k - w_2 p) \right] &= f_P p^\mu, \quad p^2 = m_P^2, \\ N_c g_V \int \frac{d^4 k}{(2\pi)^4 i} \tilde{\Phi}_V(-k^2) \text{tr} \left[O_V^\mu S_1(k + w_1 p) \not{\epsilon}_V S_2(k - w_2 p) \right] &= m_V f_V \epsilon_V^\mu, \quad p^2 = m_V^2, \end{aligned} \quad (15)$$

where $N_c = 3$ is the number of colors. As before we have $w_i = m_{q_i}/(m_{q_1} + m_{q_2})$. Further $O_P^\mu = \gamma^\mu$ and $O_V^\mu = \gamma^\mu \gamma_5$.

The compositeness conditions (14) and the fit to the leptonic decay constants (15) provide $2n_H$ constraint equations for $2n_H + 5$ model parameters. As further constraints on the parameter space, we have decided to fit the model to the eight fundamental electromagnetic decays listed in Table II. We refer the reader to Ref. [23] for the details of the one-loop calculation of the electromagnetic decays. The results of the (overconstrained) least-squares fit to the leptonic decay constants and the electromagnetic decay widths and the corresponding experimental/theoretical input values can be found in Tables I and Table II, respectively. The agreement between the fit values and input values is quite satisfactory.

The results of the fit for the values of quark masses m_{q_i} , the infrared cutoff parameter λ and the size parameters Λ_{H_i} are given in Eqs. (16), (17) and (18), respectively.

$$\begin{array}{ccccc} m_u & m_s & m_c & m_b & \lambda \\ \hline 0.235 & 0.424 & 2.16 & 5.09 & 0.181 \text{ GeV} \end{array} \quad (16)$$

$$\begin{array}{ccccccc} \Lambda_\pi & \Lambda_K & \Lambda_D & \Lambda_{D_s} & \Lambda_B & \Lambda_{B_s} & \Lambda_{B_c} & \Lambda_\rho \\ \hline 0.87 & 1.04 & 1.47 & 1.57 & 1.88 & 1.95 & 2.42 & 0.61 \text{ GeV} \end{array} \quad (17)$$

TABLE II: Input values for some basic electromagnetic decay widths and our least-squares fit values (in keV).

Process	Fit Values	Data [29]
$\pi^0 \rightarrow \gamma\gamma$	5.06×10^{-3}	$(7.7 \pm 0.4) \times 10^{-3}$
$\eta_c \rightarrow \gamma\gamma$	1.61	1.8 ± 0.8
$\rho^\pm \rightarrow \pi^\pm \gamma$	76.0	67 ± 7
$\omega \rightarrow \pi^0 \gamma$	672	703 ± 25
$K^{*\pm} \rightarrow K^\pm \gamma$	55.1	50 ± 5
$K^{*0} \rightarrow K^0 \gamma$	116	116 ± 10
$D^{*\pm} \rightarrow D^\pm \gamma$	1.22	1.5 ± 0.5
$J/\psi \rightarrow \eta_c \gamma$	1.43	1.58 ± 0.37

Λ_ω	Λ_ϕ	$\Lambda_{J/\psi}$	Λ_{K^*}	Λ_{D^*}	$\Lambda_{D_s^*}$	Λ_{B^*}	$\Lambda_{B_s^*}$	
0.47	0.88	1.48	0.72	1.16	1.17	1.72	1.71	GeV

(18)

The constituent quark masses and the values of the size parameter fall into the expected range. The size parameters show the expected general pattern in that the geometrical sizes of the mesons $\propto \Lambda_{H_i}^{-1}$ shrink as their masses increase.

The present numerical least-squares fit and the values for the model parameters supersede the results of a similar analysis given in [23] which used a different set of electromagnetic decays in the fit. In the present fit we have also updated some of the theoretical/experimental input values.

IV. TRANSITION FORM FACTORS

Given the fact that all model parameters have been fixed, the covariant quark model can now be utilized to calculate any given decay process in a parameter-free way. As a first application we calculate the form factors describing the transitions of heavy $B(B_s)$ mesons into light mesons, e.g. $B, B_s \rightarrow \pi, K, \rho, K^*, \phi$. These quantities are of great interest due to their applications in semileptonic, nonleptonic and rare decays of the B and B_s mesons. They have been calculated within the LCSR approach in the region of large recoil (small momentum transfer) and have been extrapolated to the low recoil region. Our approach allows one to evaluate the form factors in the full kinematical range including the near-zero recoil region.

Below, we list the definitions of the dimensionless invariant transition form factors together with the covariant quark model expressions that allow one to calculate them. We closely follow the notation used in our papers [19].

$$\begin{aligned}
& \langle P'_{[\bar{q}_3 q_2]}(p_2) | \bar{q}_2 O^\mu q_1 | P_{[\bar{q}_3 q_1]}(p_1) \rangle \\
&= N_c g_P g_{P'} \int \frac{d^4 k}{(2\pi)^4 i} \tilde{\Phi}_P \left(-(k + w_{13})^2 \right) \tilde{\Phi}_{P'} \left(-(k + w_{23})^2 \right) \text{tr} \left[O^\mu S_1(k + p_1) \gamma^5 S_3(k) \gamma^5 S_2(k + p_2) \right] \\
&= F_+(q^2) P^\mu + F_-(q^2) q^\mu,
\end{aligned} \tag{19}$$

$$\begin{aligned}
& \langle P'_{[\bar{q}_3 q_2]}(p_2) | \bar{q}_2 (\sigma^{\mu\nu} q_\nu) q_1 | P_{[\bar{q}_3 q_1]}(p_1) \rangle = \\
&= N_c g_P g_{P'} \int \frac{d^4 k}{(2\pi)^4 i} \tilde{\Phi}_P \left(-(k + w_{13})^2 \right) \tilde{\Phi}_{P'} \left(-(k + w_{23})^2 \right) \text{tr} \left[\sigma^{\mu\nu} q_\nu S_1(k + p_1) \gamma^5 S_3(k) \gamma^5 S_2(k + p_2) \right] \\
&= \frac{i}{m_1 + m_2} (q^2 P^\mu - q \cdot P q^\mu) F_T(q^2),
\end{aligned} \tag{20}$$

$$\begin{aligned}
& \langle V(p_2, \epsilon_2)_{[\bar{q}_3 q_2]} | \bar{q}_2 O^\mu q_1 | P_{[\bar{q}_3 q_1]}(p_1) \rangle \\
&= N_c g_P g_V \int \frac{d^4 k}{(2\pi)^4 i} \tilde{\Phi}_P \left(-(k + w_{13})^2 \right) \tilde{\Phi}_V \left(-(k + w_{23})^2 \right) \text{tr} \left[O^\mu S_1(k + p_1) \gamma^5 S_3(k) \not{\epsilon}_2^\dagger S_2(k + p_2) \right] \\
&= \frac{\epsilon_\nu^\dagger}{m_1 + m_2} \left(-g^{\mu\nu} P \cdot q A(q^2) + P^\mu P^\nu A_+(q^2) + q^\mu P^\nu A_-(q^2) + i \varepsilon^{\mu\nu\alpha\beta} P_\alpha q_\beta V(q^2) \right), \tag{21}
\end{aligned}$$

$$\begin{aligned}
& \langle V(p_2, \epsilon_2)_{[\bar{q}_3 q_2]} | \bar{q}_2 (\sigma^{\mu\nu} q_\nu (1 + \gamma^5)) q_1 | P_{[\bar{q}_3 q_1]}(p_1) \rangle \\
&= N_c g_P g_V \int \frac{d^4 k}{(2\pi)^4 i} \tilde{\Phi}_P \left(-(k + w_{13})^2 \right) \tilde{\Phi}_V \left(-(k + w_{23})^2 \right) \text{tr} \left[(\sigma^{\mu\nu} q_\nu (1 + \gamma^5)) S_1(k + p_1) \gamma^5 S_3(k) \not{\epsilon}_2^\dagger S_2(k + p_2) \right] \\
&= \epsilon_\nu^\dagger \left(-(g^{\mu\nu} - q^\mu q^\nu / q^2) P \cdot q a_0(q^2) + (P^\mu P^\nu - q^\mu P^\nu P \cdot q / q^2) a_+(q^2) + i \varepsilon^{\mu\nu\alpha\beta} P_\alpha q_\beta g(q^2) \right). \tag{22}
\end{aligned}$$

We use $P = p_1 + p_2$ and $q = p_1 - p_2$ and the on-shell conditions $\epsilon_2^\dagger \cdot p_2 = 0$, $p_i^2 = m_i^2$. Since there are three quark species involved in the transition, we have introduced a two-subscript notation $w_{ij} = m_{q_j} / (m_{q_i} + m_{q_j})$ ($i, j = 1, 2, 3$) such that $w_{ij} + w_{ji} = 1$. The form factors defined in Eq. (22) satisfy the physical requirement $a_0(0) = a_+(0)$, which ensures that no kinematic singularity appears in the matrix element at $q^2 = 0$. For reference, it is useful to relate the above form factors to those used in Ref. [9]. The relations read

$$\begin{aligned}
F_+ &= f_+, \quad F_- = -\frac{m_1^2 - m_2^2}{q^2} (f_+ - f_0), \quad F_T = f_T, \\
A_0 &= \frac{m_1 + m_2}{m_1 - m_2} A_1, \quad A_+ = A_2, \quad A_- = \frac{2m_2(m_1 + m_2)}{q^2} (A_3 - A_0), \quad V = V, \\
a_0 &= T_2, \quad g = T_1, \quad a_+ = T_2 + \frac{q^2}{m_1^2 - m_2^2} T_3. \tag{23}
\end{aligned}$$

The form factors (23) satisfy the constraints

$$\begin{aligned}
A_0(0) &= A_3(0) \\
2m_2 A_3(q^2) &= (m_1 + m_2) A_1(q^2) - (m_1 - m_2) A_2(q^2). \tag{24}
\end{aligned}$$

In Figs. 1-4, we plot our calculated form factors in the entire kinematical range $0 \leq q^2 \leq q_{\text{max}}^2$. For comparison, we also show the results obtained from the light-cone sum rules analysis [8]. In Table III, we collect our predictions for the form factors at the maximum recoil point $q^2 = 0$ and provide a comparison with results obtained within other approaches. The figures and tables highlight the wide range of phenomena accessible within our approach.

As was suggested in Ref. [11], one can check how well the quark-model form factors satisfy the three low recoil relations derived in Ref. [10] involving the pairs of form factors (T_1, V) , (T_2, A_1) , and (T_3, A_2) . In Fig. 5, we plot the ratios

$$R_1 = \frac{T_1(q^2)}{V(q^2)}, \quad R_2 = \frac{T_2(q^2)}{A_1(q^2)}, \quad R_3 = \frac{q^2}{m_B^2} \frac{T_3(q^2)}{A_2(q^2)}. \tag{25}$$

which in the heavy-quark symmetry limit and at low recoil, should all be of the order $1 - (2\alpha_s / (3\pi) \ln(\mu / m_b))$, i.e. close to one. Figure 5 shows that, similar to the extrapolated LCSR form factors, the covariant quark model form factors satisfy the low-recoil heavy-quark symmetry relations reasonably well for R_1 and R_2 but not for R_3 . Note that the q^2 scale has changed in Fig. 5.

It is interesting to compare the q^2 behavior of the $B - \pi$ transition form factors calculated from the three-point one-loop diagram with the q^2 behavior of the vector-dominance model (VDM). For example, in a monopole ansatz for the form factor $F_+^{B\pi}(q^2)$ one would have the VDM q^2 behavior

$$F_{\text{VDM}}^{B\pi}(q^2) = \frac{F_+^{B\pi}(0)}{m_{B^*}^2 - q^2}.$$

where the pole mass is given by the mass of the lowest-lying vector meson state B^* . The two curves are plotted in Fig. 6. One observes a strong rise of the VDM form factor towards the larger q^2 values close to the position of the B^* pole. A similar rise is observed for the quark-model form factor. It is quite intriguing and gratifying that the quark-model form factor is able to emulate the pole-type behavior of the VDM form factor including even the correct scale $m_{B^*}^2$ of the pole-type enhancement.

TABLE III: $q^2 = 0$ results for the transition form factors in various model approaches.

	This work	LCSR-1 [8]	LCSR-2 [9]	DSE [12]	QCD SR [17]	DQM [13]	RQM [14]	RCQM [18]
$F_+^{B\pi}(0)$	0.29	0.258±0.031	0.25±0.05	0.24±0.05	0.24±0.03	0.29	0.22	0.27
$F_+^{BK}(0)$	0.42	0.335±0.042	0.31±0.04	0.30±0.06	0.25±0.03	0.36		0.36
$F_T^{B\pi}(0)$	0.27	0.253±0.028	0.21±0.04	0.25±0.05		0.28		
$F_T^{BK}(0)$	0.40	0.359±0.038	0.27±0.04	0.32±0.06	0.14±0.03	0.35		0.34
$V^{B\rho}(0)$	0.28	0.324±0.029	0.32±0.10	0.31±0.06		0.31	0.30	
$V^{BK^*}(0)$	0.36	0.412±0.045	0.39±0.11	0.37±0.07	0.47±0.03	0.44		
$V^{B_s\phi}(0)$	0.32	0.434±0.035						
$A_1^{B\rho}(0)$	0.26	0.240±0.024	0.24±0.08	0.24±0.05		0.26	0.27	
$A_1^{BK^*}(0)$	0.33	0.290±0.036	0.30±0.08	0.29±0.06	0.37±0.03	0.36		
$A_1^{B_s\phi}(0)$	0.29	0.311±0.029						
$A_2^{B\rho}(0)$	0.24	0.221±0.023	0.21±0.09	0.25±0.05		0.24	0.28	
$A_2^{BK^*}(0)$	0.32	0.258±0.035	0.26±0.08	0.30±0.06	0.40±0.03	0.32		
$A_2^{B_s\phi}(0)$	0.28	0.234±0.028						
$T_1^{B\rho}(0)$	0.25	0.268±0.021	0.28±0.09	0.26±0.05		0.27		
$T_1^{BK^*}(0)$	0.33	0.332±0.037	0.33±0.10	0.30±0.06	0.19±0.03	0.39		
$T_1^{B_s\phi}(0)$	0.28	0.349±0.033						

V. NONLEPTONIC B_s DECAYS

As a second application we consider the two-body nonleptonic B_s decays $B_s \rightarrow D_s^{(*)-} D_s^{(*)+}$ and $B_s \rightarrow J/\psi\phi$, which have recently attracted some interest. The modes $D_s^- D_s^+$, $D_s^{*-} D_s^+ + D_s^- D_s^{*+}$, and $D_s^{*-} D_s^{*+}$ give the largest contribution to $\Delta\Gamma$ for the $B_s - \bar{B}_s$ system. The mode $J/\psi\phi$ is color-suppressed but it is interesting for the search of possible CP-violating new physics effects in $B_s - \bar{B}_s$ mixing.

It is convenient to express all physical observables in terms of helicity form factors H_m . This will result in very compact rate expressions. Furthermore, in the case of the two-vector meson decays $P \rightarrow VV$, the helicity representation is quite convenient since one can then easily calculate the helicity composition of the rate $\Gamma_L, \Gamma_-, \Gamma_+$.

The helicity form factors H_m can be expressed in terms of the invariant form factors of Ref. [9] in the following way [19]:

(a) Spin $S = 0$:

$$\begin{aligned}
 H_t &= \frac{1}{\sqrt{q^2}} \{ (m_1^2 - m_2^2) F_+ + q^2 F_- \} , \\
 H_0 &= \frac{2m_1 |\mathbf{p}_2|}{\sqrt{q^2}} F_+ .
 \end{aligned}
 \tag{26}$$

(b) Spin $S = 1$:

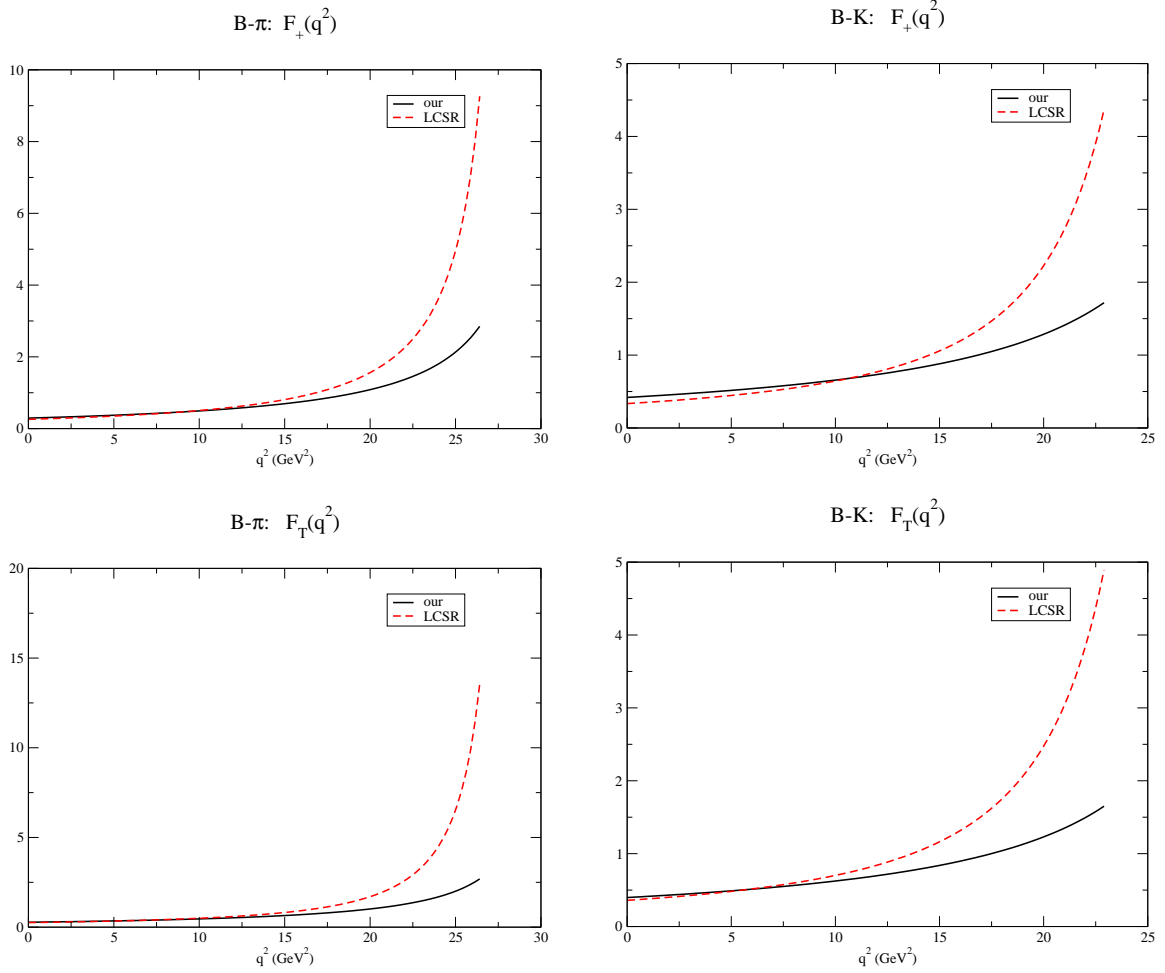


FIG. 1: Our results for the form factors appearing in Eqs. (19) and (20) – *Left panel*, $B - \pi$ -transition; and *right panel*, $B - K$ -transition. For comparison, we plot the corresponding LCSR curves from Ref. [8].

$$\begin{aligned}
 H_t &= \frac{1}{m_1 + m_2} \frac{m_1 |\mathbf{p}_2|}{m_2 \sqrt{q^2}} \{ (m_1^2 - m_2^2) (A_+ - A_0) + q^2 A_- \}, \\
 H_{\pm} &= \frac{1}{m_1 + m_2} \{ -(m_1^2 - m_2^2) A_0 \pm 2 m_1 |\mathbf{p}_2| V \}, \\
 H_0 &= \frac{1}{m_1 + m_2} \frac{1}{2 m_2 \sqrt{q^2}} \{ -(m_1^2 - m_2^2) (m_1^2 - m_2^2 - q^2) A_0 + 4 m_1^2 |\mathbf{p}_2|^2 A_+ \},
 \end{aligned} \tag{27}$$

where $|\mathbf{p}_2| = \lambda^{1/2}(m_1^2, m_2^2, q^2)/(2 m_1)$ is the momentum of the outgoing particles in the rest frame of the decaying particle.

The effective Hamiltonian describing the B_s nonleptonic decays is given by (see Ref. [4])

$$\begin{aligned}
 \mathcal{H}_{\text{eff}} &= -\frac{G_F}{\sqrt{2}} V_{cb} V_{cs}^\dagger \sum_{i=1}^6 C_i Q_i, \\
 Q_1 &= (\bar{c}_{a_1} b_{a_2})_{V-A} (\bar{s}_{a_2} c_{a_1})_{V-A}, & Q_2 &= (\bar{c}_{a_1} b_{a_1})_{V-A}, (\bar{s}_{a_2} c_{a_2})_{V-A}, \\
 Q_3 &= (\bar{s}_{a_1} b_{a_1})_{V-A} (\bar{c}_{a_2} c_{a_2})_{V-A}, & Q_4 &= (\bar{s}_{a_1} b_{a_2})_{V-A} (\bar{c}_{a_2} c_{a_1})_{V-A}, \\
 Q_5 &= (\bar{s}_{a_1} b_{a_1})_{V-A} (\bar{c}_{a_2} c_{a_2})_{V+A}, & Q_6 &= (\bar{s}_{a_1} b_{a_2})_{V-A} (\bar{c}_{a_2} c_{a_1})_{V+A},
 \end{aligned} \tag{28}$$

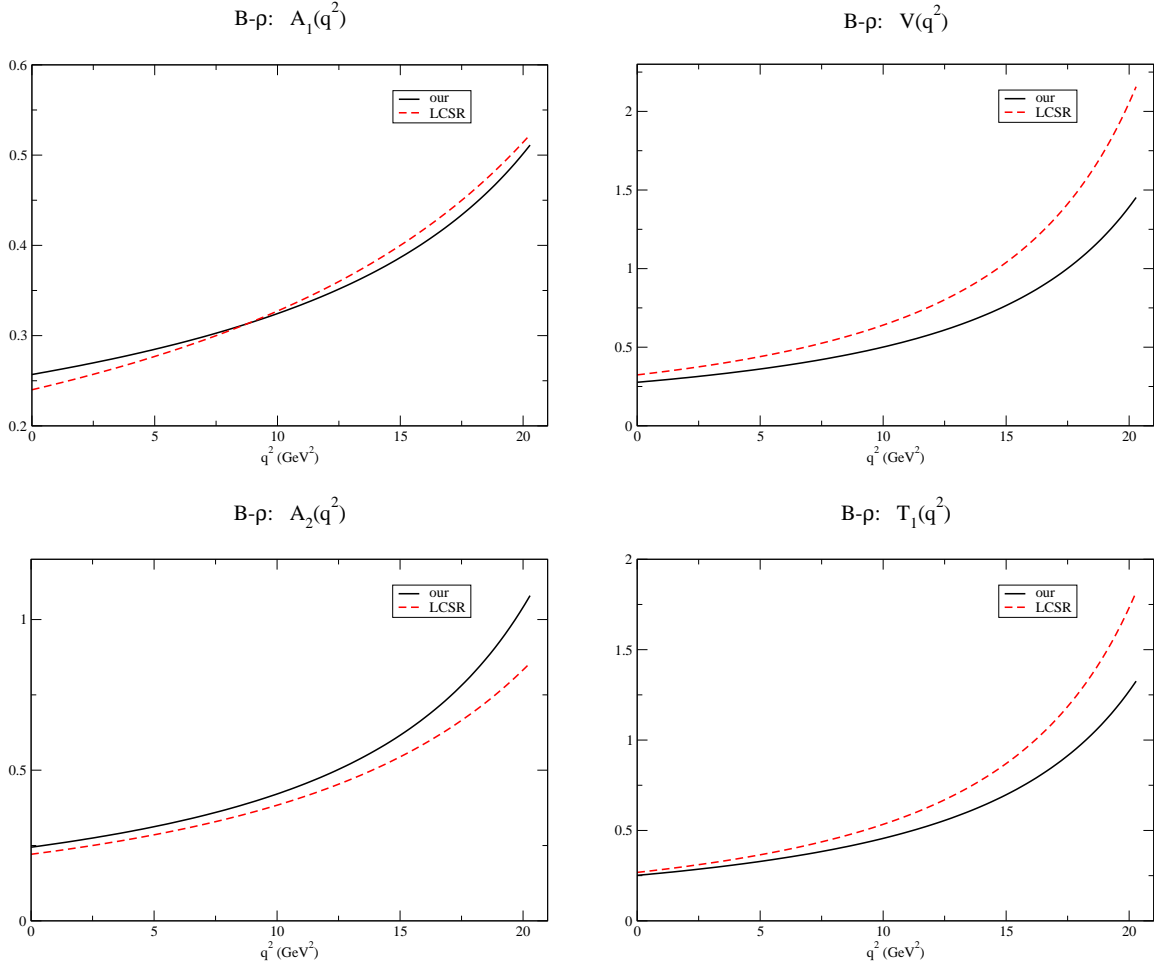


FIG. 2: Our results for the form factors appearing in Eqs. (21) and (22) for $B - \rho$ transition. For comparison, we plot the corresponding LCSR curves from Ref. [8].

where the subscript $V - A$ refers to the usual left-chiral current $O_-^\mu = \gamma^\mu(1 - \gamma^5)$ and $V + A$ to the usual right-chiral one $O_+^\mu = \gamma^\mu(1 + \gamma^5)$. The a_i denote color indices. We calculate the nonleptonic B_s -decay widths by using *naive* factorization. In this paper we consider the following nonleptonic decays of the B_s -meson:

$$B_s(p) \rightarrow D_s^-(q_1)D_s^{*+}(q_2), D_s^-(q_1)D_s^{*+}(q_2, \epsilon_2), D_s^{*-}(q_1, \epsilon_1)D_s^+(q_2), D_s^{*-}(q_1, \epsilon_1)D_s^{*+}(q_2, \epsilon_2), \text{ and } J/\psi(q_1, \epsilon_1)\phi(q_2, \epsilon_2).$$

The widths can be conveniently expressed in terms of the helicity form factors and leptonic decay constants. In the case of the color-allowed decays $B_s \rightarrow D_s^{(*)-}D_s^{(*)+}$ one has

$$\begin{aligned} \Gamma(B_s \rightarrow D_s^- D_s^+) &= \frac{G_F^2 |\mathbf{q}_2|}{16\pi m_{B_s}^2} [\lambda_c^{(s)}]^2 \left(C_2^{\text{eff}} m_{D_s} f_{D_s} H_t^{B_s D_s}(m_{D_s}^2) + 2 C_6^{\text{eff}} f_{D_s}^{PS} F_S^{B_s D_s}(m_{D_s}^2) \right)^2, \\ \Gamma(B_s \rightarrow D_s^- D_s^{*+}) &= \frac{G_F^2 |\mathbf{q}_2|}{16\pi m_{B_s}^2} [\lambda_c^{(s)}]^2 \left(C_2^{\text{eff}} m_{D_s} f_{D_s} H_t^{B_s D_s^*}(m_{D_s}^2) + 2 C_6^{\text{eff}} \frac{m_{B_s} |\mathbf{q}_2|}{m_{D_s^*}} f_{D_s}^{PS} F_{PS}^{B_s D_s^*}(m_{D_s}^2) \right)^2, \\ \Gamma(B_s \rightarrow D_s^{*-} D_s^+) &= \frac{G_F^2 |\mathbf{q}_2|}{16\pi m_{B_s}^2} [\lambda_c^{(s)}]^2 \left(C_2^{\text{eff}} m_{D_s^*} f_{D_s^*} H_0^{B_s D_s^*}(m_{D_s^*}^2) \right)^2, \\ \Gamma(B_s \rightarrow D_s^{*-} D_s^{*+}) &= \frac{G_F^2 |\mathbf{q}_2|}{16\pi m_{B_s}^2} [\lambda_c^{(s)}]^2 (C_2^{\text{eff}} m_{D_s^*} f_{D_s^*})^2 \sum_{i=0, \pm} \left(H_i^{B_s D_s^*}(m_{D_s^*}^2) \right)^2. \end{aligned} \quad (29)$$

Here, $\lambda_c^{(s)} = \frac{G_F}{\sqrt{2}} |V_{cb} V_{cs}^\dagger|$. The Wilson coefficients appear in the combinations $C_2^{\text{eff}} = C_2 + \xi C_1 + C_4 + \xi C_3$ and $C_6^{\text{eff}} = C_6 + \xi C_5$, where terms multiplied by the color factor $\xi = 1/N_c$ will be dropped in the numerical calculations

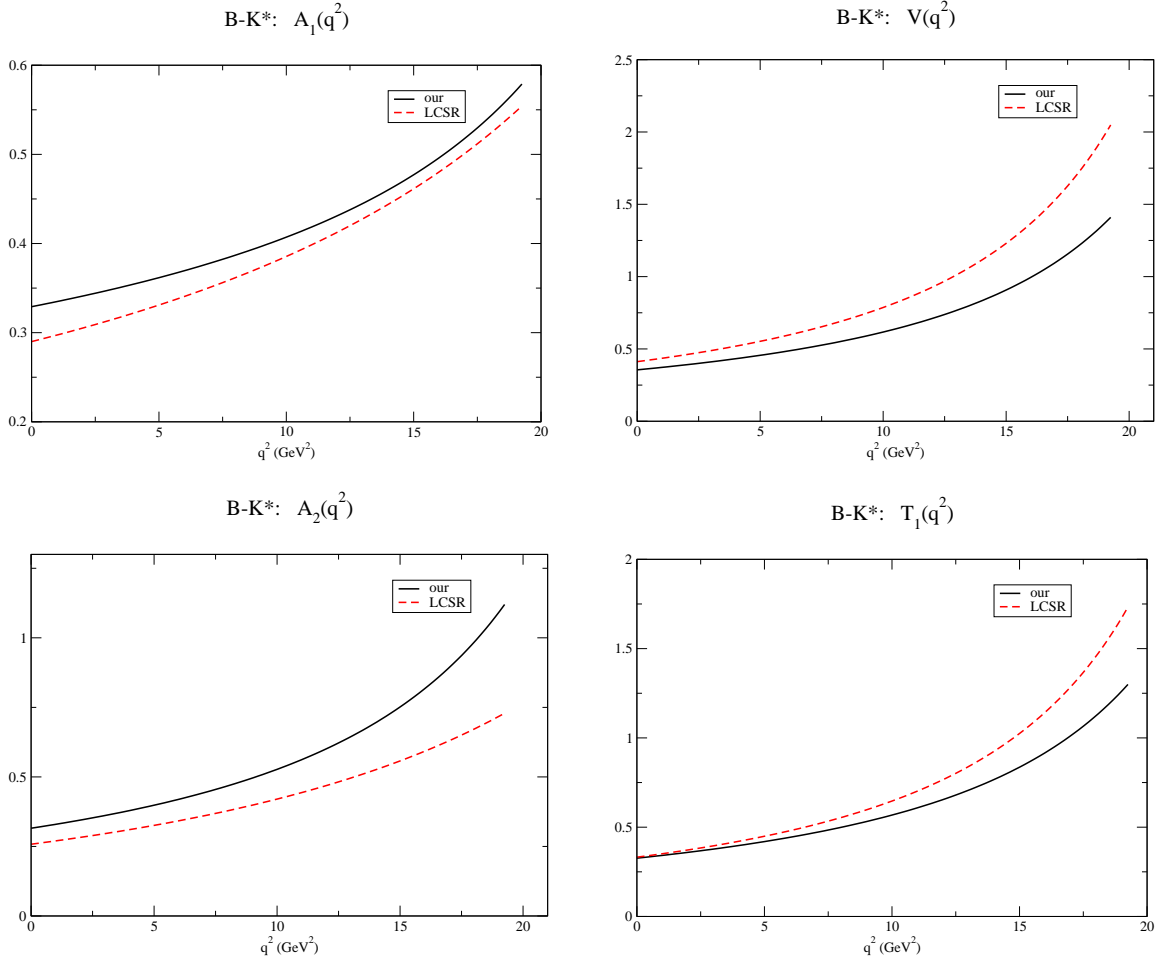


FIG. 3: Our results for the form factors appearing in Eqs. (21) and (22) for $B - K^*$ transition. For comparison, we plot the corresponding LCSR curves from Ref. [8].

according to the $1/N_c$ -expansion. The annihilation channels that also contribute to the above color-allowed decays will be neglected since they are color and form factor suppressed.

The width of the color-suppressed $B_s \rightarrow J/\psi \phi$ decay is written as

$$\Gamma(B_s \rightarrow J/\psi \phi) = \frac{G_F^2 |\mathbf{q}_2|}{16\pi m_{B_s}^2} [\lambda_c^{(s)}]^2 (C_1^{\text{eff}} + C_5^{\text{eff}})^2 (m_{J/\psi} f_{J/\psi})^2 \sum_{i=0,\pm} \left(H_i^{B_s J/\psi}(m_{J/\psi}^2) \right)^2, \quad (30)$$

where we have combined the Wilson coefficients into $C_1^{\text{eff}} = C_1 + \xi C_2 + C_3 + \xi C_4$ and $C_5^{\text{eff}} = C_5 + \xi C_6$.

For the Cabibbo-Kobayashi-Maskawa-matrix elements, we use the values from Ref. [29]:

$ V_{ud} $	$ V_{us} $	$ V_{ub} $	$ V_{cd} $	$ V_{cs} $	$ V_{cb} $
0.974	0.225	0.00389	0.230	0.975	0.0406

(31)

For the values of the Wilson coefficients we take [34]

C_1	C_2	C_3	C_4	C_5	C_6
-0.257	1.009	-0.005	-0.078	0.000	0.001

(32)

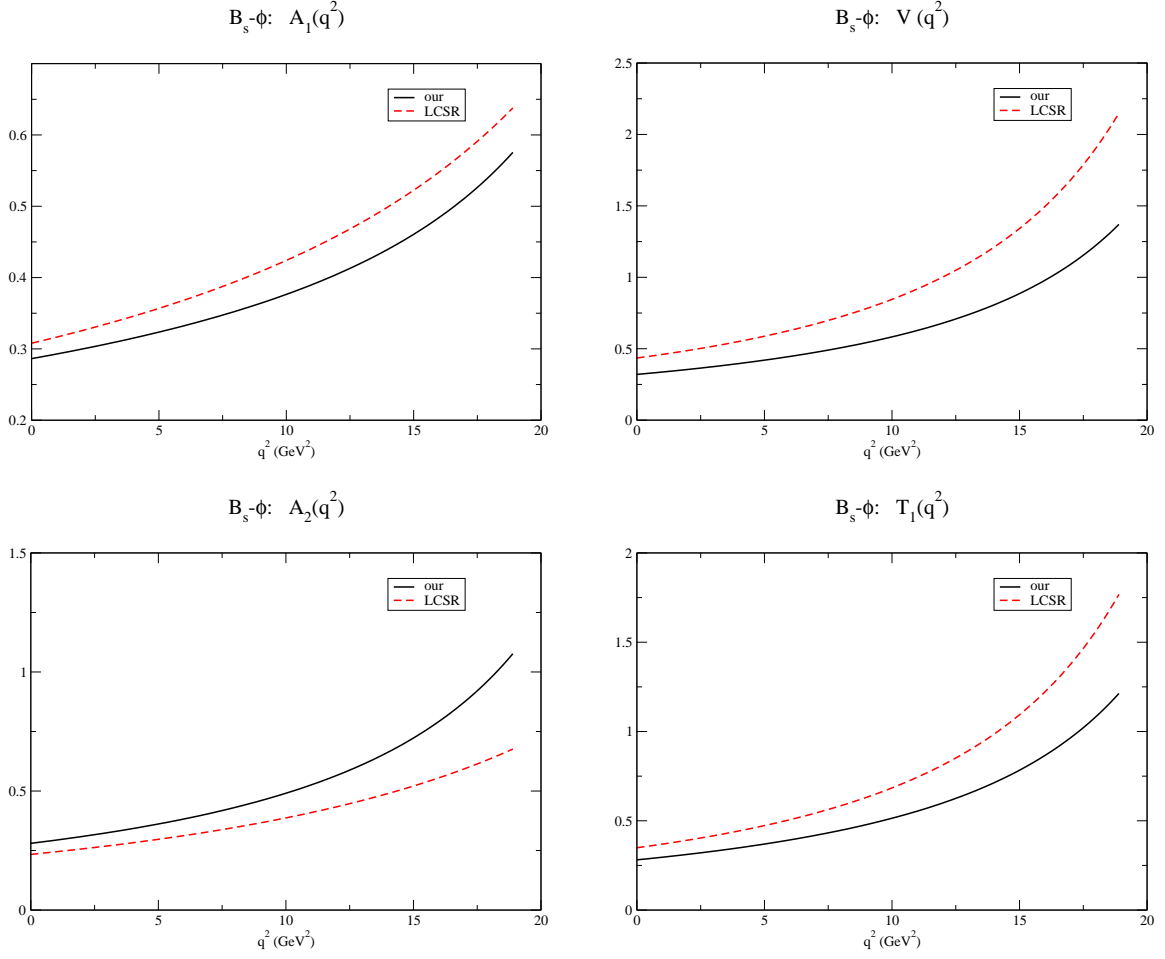


FIG. 4: Our results for the form factors appearing in Eqs. (21) and (22) for $B_s - \phi$ transition. For comparison, we plot the corresponding LCSR curves from Ref. [8].

evaluated to next-to-next-to leading logarithmic accuracy in the \overline{MS} (NDR) renormalization scheme at the scale $\mu = 4.8$ GeV [35].

We also need the values of the $B_s - \phi$ transition form factors evaluated at $q^2 = m_{J/\psi}^2$. They are given in Table IV where we compare our results with corresponding results of Ref. [3]. The agreement for the form factors $A_1(m_{J/\psi}^2)$ and $A_2(m_{J/\psi}^2)$ is satisfactory. Our value for the form factor $V(m_{J/\psi}^2)$ is somewhat smaller than the one found in Ref. [3].

TABLE IV: The relevant $B_s - \phi$ form factors at $q^2 = m_{J/\psi}^2$ calculated in this work. For comparison, we give the results of Ref. [3].

	This work	Ref. [3]
$A_1(m_{J/\psi}^2)$	0.37	0.42 ± 0.06
$A_2(m_{J/\psi}^2)$	0.48	0.38 ± 0.06
$V(m_{J/\psi}^2)$	0.56	0.82 ± 0.12

In Table V we give our results for the branching ratios. One can see that there is good agreement with the available experimental data.

We finally give our results on the helicity fractions in the two decays $B_s \rightarrow D_s^{*-} D_s^{*+}$ and $B_s \rightarrow J/\psi \phi$. The helicity

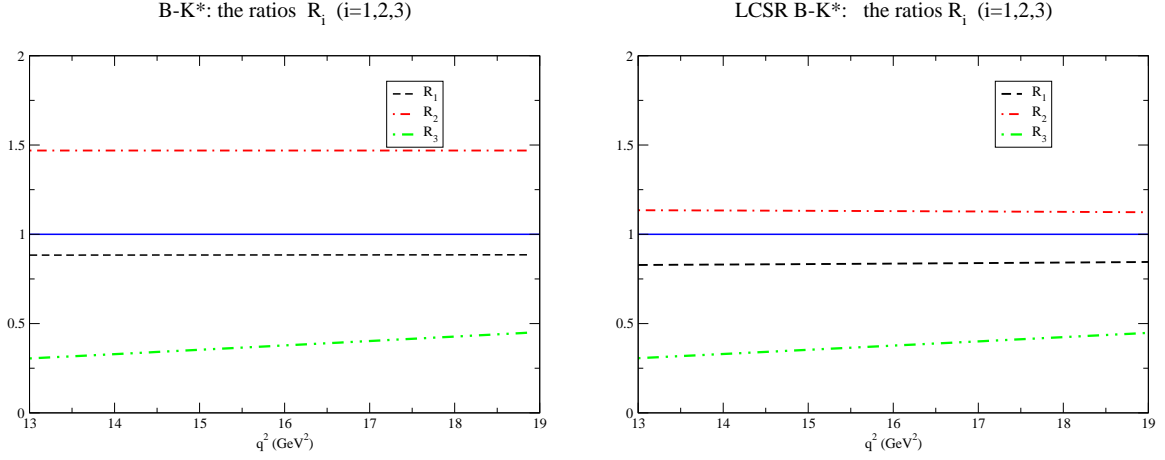


FIG. 5: Our results for the ratios of the form factors appearing in Eq. (25) for $B - K^*$ -transition.

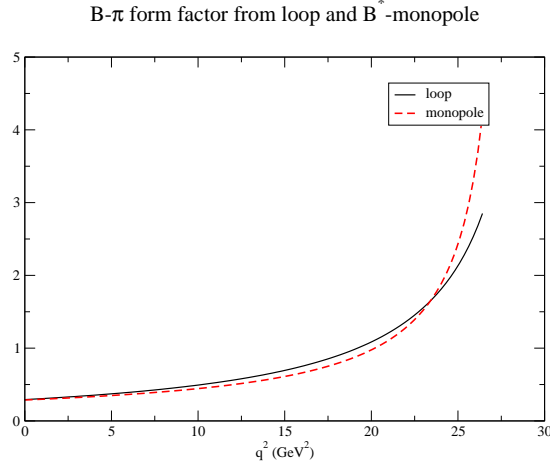


FIG. 6: Comparison of the $B - \pi$ - form factors obtained from the covariant quark model and from a VDM-monopole ansatz.

fractions of the nonleptonic $B_s \rightarrow VV$ rates are defined as

$$\hat{\Gamma}_L = \frac{|H_0|^2}{|H_0|^2 + |H_+|^2 + |H_-|^2}, \quad \hat{\Gamma}_\pm = \frac{|H_\pm|^2}{|H_0|^2 + |H_+|^2 + |H_-|^2}, \quad \hat{\Gamma}_\perp = \frac{1}{2} \frac{|H_+ - H_-|^2}{|H_0|^2 + |H_+|^2 + |H_-|^2}. \quad (33)$$

Note that we have normalized the partial helicity rates to the total rate such that one has $(\hat{\Gamma}_L + \hat{\Gamma}_- + \hat{\Gamma}_+) = 1$. For $B_s \rightarrow D_s^{*-} D_s^{*+}$ we find $(\hat{\Gamma}_L, \hat{\Gamma}_-, \hat{\Gamma}_+) = (0.549, 0.366, 0.0847)$ and for $B_s \rightarrow J/\psi \phi$ we find $(0.420, 0.552, 0.0272)$. The hierarchy of partial helicity rates $\hat{\Gamma}_L > \hat{\Gamma}_- > \hat{\Gamma}_+$ seen in the decay $B_s \rightarrow D_s^{*-} D_s^{*+}$ is expected for tree-level-dominated nonleptonic decays using simple on-shell quark model arguments. One finds that, at the leading order of $m_1 = m_{B_s}$, the partial rate Γ_- is helicity-suppressed by the factor $4q^2/m_1^2$ with $q^2 = m_{D_s^{*+}}^2$ and the partial rate Γ_+ is further chirality suppressed by the factor m_2^2/m_1^2 with $m_2 = m_{D_s^{*+}}$ in addition to the helicity suppression [36–38]. Using the qualitative suppression factors one finds $(0.583, 0.361, 0.056)$ for the helicity fractions in the decay $B_s \rightarrow D_s^{*-} D_s^{*+}$ which is remarkably close to the results of the full calculation. For the process $B_s \rightarrow J/\psi \phi$ with a larger q^2 -value of $q^2 = m_{J/\psi}^2$ the helicity suppression is no longer in effect since now $4q^2/m_1^2 = 1.332$. One now obtains $(0.420, 0.560, 0.020)$ for the helicity fractions which again is remarkably close to the results of the full calculation. One has an inversion of the hierarchy for the longitudinal and transverse-minus rates for $B_s \rightarrow J/\psi \phi$ in as much as one now has $\hat{\Gamma}_L < \hat{\Gamma}_-$. Experimental numbers on the partial helicity rates exist only for the decay $B_s \rightarrow J/\psi \phi$ given by $\hat{\Gamma}_L = 0.541 \pm 0.017$ and $\hat{\Gamma}_\perp = 0.241 \pm 0.023$ [29]. Our calculated longitudinal rate can be seen to be off by several standard deviations. In order to be able to compare with the experimental transverse rate $\hat{\Gamma}_\perp$ one needs to use

TABLE V: Branching ratios (%) of the B_s nonleptonic decays calculated in our approach.

Process	This work	Exp. data [29]
$B_s \rightarrow D_s^- D_s^+$	1.65	$1.04^{+0.29}_{-0.26}$
$B_s \rightarrow D_s^- D_s^{*+} + D_s^{*-} D_s^+$	2.40	2.8 ± 1.0
$B_s \rightarrow D_s^{*-} D_s^{*+}$	3.18	3.1 ± 1.4
$B_s \rightarrow J/\psi \phi$	0.16	0.14 ± 0.05

$\Gamma_\perp \propto |A_\perp|^2 = |H_+ - H_-|^2/2$. For $B_s \rightarrow D_s^{*-} D_s^{*+}$ we find $\hat{\Gamma}_\perp = 0.0493$ and for $B_s \rightarrow J/\psi \phi$ we predict $\hat{\Gamma}_\perp = 0.167$. Again we are off the experimental result by several standard deviations.

VI. SUMMARY

We have given a brief sketch of the theoretical framework underlying the covariant quark model, including a discussion of how infrared confinement is incorporated in the model. We have discussed in some detail how the model parameters of the covariant quark model are determined through a least-squares fit to experimental/theoretical data on the leptonic decay constants and eight fundamental mesonic one- and two-photon decays. Once the model parameters of the covariant quark model are fixed the model can be used to obtain parameter-free predictions for any transition process involving light or heavy mesons.

In the present paper, we have calculated the transition form factors of the heavy B and B_s mesons to light pseudoscalar and vector mesons, which are needed as ingredients for the calculation of the semileptonic, nonleptonic, and rare decays of the B and B_s mesons. Our form factor results hold in the full kinematical range of momentum transfer. We have provided a detailed discussion of how the covariant-quark-model form factors compare with the corresponding LCSR form factors.

We have finally made use of the calculated form factors to calculate the nonleptonic decays $B_s \rightarrow D_s^{(*)-} D_s^{(*)+}$ and $B_s \rightarrow J/\psi \phi$, which have been widely discussed recently in the context of $B_s - \bar{B}_s$ -mixing and CP violation. We have also presented results on the helicity composition for the decays $B_s \rightarrow VV$. Further application of our form factor results are envisaged, such as the calculation of the penguin-dominated decay $B_s \rightarrow K^{(*)} \bar{K}^{(*)}$.

Acknowledgments

This work was supported by the DFG Grant No. KO 1069/13-1, the Heisenberg-Landau program, Russian Fund of Basic Research Grant No. 10-02-00368-a, FONDECYT projects 1100582 and Centro-Científico-Tecnológico de Valparaíso PBCT ACT-028.

-
- [1] S Stone, "Heavy Flavor Physics", [arXiv:1109.3361 [hep-ph]]. To appear in Proceedings of the DPF-2011 Conference, Providence, RI, August 8-13, 2011.
 - [2] B. El-Bennich, J. P. B. C. de Melo, O. Leitner, B. Loiseau, J.-P. Dedonder, [arXiv:1111.6955 [hep-ph]], in Erice School on Nuclear Physics 2011: From Quarks and Gluons to Hadrons and Nuclei (unpublished).
 - [3] S. Faller, R. Fleischer, T. Mannel, Phys. Rev. **D79**, 014005 (2009). [arXiv:0810.4248 [hep-ph]].
 - [4] G. Buchalla, A. J. Buras, M. E. Lautenbacher, Rev. Mod. Phys. **68**, 1125-1144 (1996). [hep-ph/9512380].
 - [5] M. Beneke, G. Buchalla, M. Neubert and C. T. Sachrajda, Phys. Rev. Lett. **83**, 1914 (1999) [hep-ph/9905312]; M. Beneke, M. Neubert, Nucl. Phys. **B675**, 333-415 (2003). [hep-ph/0308039].
 - [6] T. Feldmann, "Soft-Collinear Effective Theory: Recent Results and Applications," PoS **CONFINEMENT8**, 007 (2008). [arXiv:0811.4590 [hep-ph]].
 - [7] C. W. Bauer, S. Fleming, D. Pirjol, I. W. Stewart, Phys. Rev. **D63**, 114020 (2001). [hep-ph/0011336].
 - [8] P. Ball and R. Zwicky, Phys. Rev. D **71**, 014029 (2005) [arXiv:hep-ph/0412079].
 - [9] A. Khodjamirian, T. Mannel, N. Offen, Phys. Rev. **D75**, 054013 (2007). [hep-ph/0611193].
 - [10] B. Grinstein, D. Pirjol, Phys. Rev. **D70**, 114005 (2004). [hep-ph/0404250].
 - [11] C. Bobeth, G. Hiller, D. van Dyk, JHEP **1007**, 098 (2010) [arXiv:1006.5013 [hep-ph]]; JHEP **1107**, 067 (2011). [arXiv:1105.0376 [hep-ph]].
 - [12] M. A. Ivanov, J. G. Körner, S. G. Kovalenko, C. D. Roberts, Phys. Rev. **D76**, 034018 (2007). [nucl-th/0703094].
 - [13] D. Melikhov, N. Nikitin and S. Simula, Phys. Rev. D **57**, 6814 (1998), [arXiv:hep-ph/9711362]; D. Melikhov, Eur. Phys. J. direct C **4**, 1 (2002), [arXiv:hep-ph/0110087].
 - [14] D. Ebert, R. N. Faustov, V. O. Galkin, Phys. Rev. **D75**, 074008 (2007). [hep-ph/0611307].
 - [15] M. Ladisa, G. Nardulli, P. Santorelli, Phys. Lett. **B455**, 283-290 (1999). [hep-ph/9903206].
 - [16] P. Colangelo, F. De Fazio, M. Ladisa, G. Nardulli, P. Santorelli and A. Tricarico, Eur. Phys. J. C **8**, 81 (1999) [hep-ph/9809372].
 - [17] P. Colangelo, F. De Fazio, P. Santorelli, E. Scrimieri, Phys. Rev. **D53**, 3672-3686 (1996). [hep-ph/9510403]; P. Colangelo, P. Santorelli, Phys. Lett. **B327**, 123-128 (1994). [hep-ph/9312258].
 - [18] A. Faessler, T. Gutsche, M. A. Ivanov, J. G. Körner and V. E. Lyubovitskij, Eur. Phys. J. direct C **4**, 18 (2002) [arXiv:hep-ph/0205287].
 - [19] M. A. Ivanov, J. G. Körner and P. Santorelli, Phys. Rev. D **63**, 074010 (2001) [arXiv:hep-ph/0007169]; Phys. Rev. D **71**, 094006 (2005) [arXiv:hep-ph/0501051]; Phys. Rev. **D73**, 054024 (2006) [hep-ph/0602050].
 - [20] M. A. Ivanov, J. G. Körner and O. N. Pakhomova, Phys. Lett. B **555**, 189 (2003) [arXiv:hep-ph/0212291].
 - [21] A. Salam, Nuovo Cim. **25**, 224 (1962); S. Weinberg, Phys. Rev. **130**, 776 (1963);
 - [22] For a review, see: K. Hayashi, M. Hirayama, T. Muta, N. Seto and T. Shirafulji, Fort. der Phys. **15**, 625 (1967).
 - [23] T. Branz, A. Faessler, T. Gutsche, M. A. Ivanov, J. G. Körner, V. E. Lyubovitskij, Phys. Rev. **D81**, 034010 (2010). [arXiv:0912.3710 [hep-ph]].
 - [24] S. Dubnicka, A. Z. Dubnickova, M. A. Ivanov, J. G. Körner, Phys. Rev. **D81**, 114007 (2010). [arXiv:1004.1291 [hep-ph]].
 - [25] S. Dubnicka, A. Z. Dubnickova, M. A. Ivanov, J. G. Körner, P. Santorelli, G. G. Saidullaeva, Phys. Rev. **D84**, 014006 (2011). [arXiv:1104.3974 [hep-ph]].
 - [26] G. V. Efimov and M. A. Ivanov, "The Quark Confinement Model Of Hadrons," *Bristol, UK: IOP (1993) 177 p*; Int. J. Mod. Phys. A **4**, 2031 (1989).
 - [27] M. A. Ivanov, M. P. Locher and V. E. Lyubovitskij, Few Body Syst. **21**, 131 (1996) [arXiv:hep-ph/9602372]; M. A. Ivanov and V. E. Lyubovitskij, Phys. Lett. B **408**, 435 (1997) [arXiv:hep-ph/9705423].
 - [28] J. A. M. Vermaseren, Nucl. Phys. Proc. Suppl. **183**, 19 (2008) [arXiv:0806.4080 [hep-ph]]; arXiv:math-ph/0010025.
 - [29] K. Nakamura *et al.* [Particle Data Group Collaboration], J. Phys. G **G37** (2010) 075021 (see also the 2011 update).
 - [30] J. L. Rosner, S. Stone, [arXiv:1002.1655 [hep-ex]].
 - [31] J. Laiho, E. Lunghi, R. S. Van de Water, Phys. Rev. **D81**, 034503 (2010). [arXiv:0910.2928 [hep-ph]].
 - [32] T. -W. Chiu *et al.* [TWQCD Collaboration], Phys. Lett. **B651**, 171-176 (2007). [arXiv:0705.2797 [hep-lat]].
 - [33] D. Becirevic, P. Boucaud, J. P. Leroy, V. Lubicz, G. Martinelli, F. Mescia, F. Rapuano, Phys. Rev. **D60**, 074501 (1999). [hep-lat/9811003].
 - [34] W. Altmannshofer, P. Ball, A. Bharucha, A. J. Buras, D. M. Straub, M. Wick, JHEP **0901**, 019 (2009). [arXiv:0811.1214 [hep-ph]].
 - [35] C. Bobeth, M. Misiak, J. Urban, Nucl. Phys. **B574**, 291-330 (2000). [hep-ph/9910220].
 - [36] J. G. Körner and G. R. Goldstein, Phys. Lett. B **89** (1979) 105.
 - [37] A. Ali, J. G. Körner, G. Kramer and J. Willrodt, Z. Phys. C **1** (1979) 269.
 - [38] M. Beneke, J. Rohrer and D. Yang, Nucl. Phys. B **774** (2007) 64 [hep-ph/0612290].
 - [39] Previously we referred to the covariant quark model as the relativistic quark model. We decided to rechristen its name in order to set it apart from other relativistic quark models as e.g. the one developed by Ebert, Faustov and Galkin [14] which contain relativistic elements but are not truly covariant.